

Fairness-Oriented User Scheduling for Bursty Downlink Transmission Using Multi-Agent Reinforcement Learning

Mingqi Yuan^{1,2}, Qi Cao¹, Man-On Pun^{†1,2,3} and Yi Chen^{1,2}

¹School of Science and Engineering, The Chinese University of Hong Kong, Shenzhen, China, 518172

²Shenzhen Research Institute of Big Data, Shenzhen, China, 518172

³Shenzhen Key Laboratory of IoT Intelligent System and Wireless Network Technology, Shenzhen, China, 518172

Abstract—In this work, we develop practical user scheduling algorithms for downlink bursty traffic with emphasis on user fairness. In contrast to the conventional scheduling algorithms that either equally divides the transmission time slots among users or maximizing some ratios without practical physical interpretations, we propose to use the 5%-tile user data rate (5TUDR) as the metric to evaluate user fairness. Since it is difficult to directly optimize 5TUDR, we first cast the problem into the stochastic game framework and subsequently propose a *Multi-Agent Reinforcement Learning* (MARL)-based algorithm to perform distributed optimization on the resource block group (RBG) allocation. Furthermore, each MARL agent is designed to take information measured by network counters from multiple network layers (e.g. Channel Quality Indicator, Buffer size) as the input *states* while the RBG allocation as *action* with a carefully designed *reward* function developed to maximize 5TUDR. Extensive simulation is performed to show that the proposed MARL-based scheduler can achieve fair scheduling while maintaining good average network throughput as compared to conventional schedulers.

Index Terms—User scheduling, RBG allocation, Fairness-oriented, Multi-Agent Reinforcement Learning (MARL)

I. INTRODUCTION

Future wireless networks have been envisaged to provide high-quality data services simultaneously to a massive number of devices [1], [2]. To accomplish this demanding goal, intensive research has been devoted to investigating how to allocate limited network resources to multiple users in an effective and yet, fair manner. In particular, user scheduling in the downlink transmission that concerns which active users should be selected and allocated network resources for transmission at the current time slot has drawn much research attention. By equally dividing the transmission time to each user, the Round Robin scheduling (RRS) can achieve the time-fairness at the cost of the network throughput [3]. In contrast, the opportunistic scheduling (OPS) was designed to allocate network resources to the advantageous users of the best instantaneous channel conditions [4]. However, OPS attains the highest network throughput by scarifying those

users of poor channel conditions, which incurs unfair resources allocation among users. To balance user fairness and network throughput, the proportional fairness scheduling (PFS) algorithm was proposed in the seminal work [5] by assigning scheduling priorities to users of the largest ratios between their instantaneous feasible data rates and achieved average data rates. Recently, [6] proposed a parameterized PFS called Generalized PFS (GPFS) by generalizing the ratio defined in PFS with different weights. However, both PFS and GPFS only take advantages of information from one single layer, i.e. the physical (PHY) layer. Since the network throughput is governed by protocols across multiple network layers, more comprehensive information from different network layers is required to better characterize the dynamics of the network throughput.

To cope with this problem, a machine learning (ML) approach has recently been proposed for user scheduling [7]. In sharp contrast to the conventional model-based approach, the data-driven ML approach exploits the massive data retrieved from the network without explicitly deriving the mathematical optimization model. In [8], a reinforcement learning (RL)-based algorithm was proposed to intelligently select the best scheduling algorithm from a set of pre-defined algorithms in each transmission time interval (TTI) based on the network conditions. Despite its good performance, the RL-based scheduler proposed in [8] suffers from large computational complexity. To circumvent this problem, [9] proposed an improved RL-based scheduler by taking into account the estimated instantaneous data rate, the averaged data rate and other metrics in constructing its input state space. More recently, [10] proposed a generative adversarial network (GAN)-empowered deep distributed RL method to allocate radio resource groups (RBGs) in a demand-aware resource management approach.

However, all the aforementioned scheduling algorithms, regardless of their model-based or data-driven nature, were established upon the assumption of full-buffer traffic, i.e. all users have infinite amount of data for downlink transmission. However, all traffic in practical networks is bursty, i.e. each user's requested data volume is finite. If bursty traffic is considered, the concept of time-fairness becomes rather non-trivial. Since it takes less transmission time slots for users of

This work was supported, in part, by the Shenzhen Institute of Artificial Intelligence and Robotics for Society (AIRS) under grant No. AC01202005001, the Shenzhen Science and Technology Innovation Committee under Grant No. JCYJ20190813170803617, and by the National Natural Science Foundation of China under Grant No. 61731018.

[†] Corresponding author, email: SimonPun@cuhk.edu.cn.

a smaller amount of bursty data to finish their transmissions in general, it is reasonable to argue that equally dividing transmission time slots among all users is unfair for users requesting for more data. As a result, the concept of time-fairness becomes very subjective for the bursty traffic case. Some pioneering works on scheduling bursty traffic were reported in the literature. In [11], two novelty concepts, namely the average user perceived throughput (UPT) and the user perceived throughput-cut (UPT-cut), were proposed to measure user fairness before a percentage proportional fair scheduling (PPFS) algorithm was devised to allocate more transmission time slots to users of a larger amount of bursty data. Furthermore, PPFS improves the average UPT by assigning higher priorities to users of less remaining transmission data. Recently, [12] proposed a hybrid downlink scheduling approach to serve bursty traffic classes of different Quality of Service (QoS) requirements. More specifically, [12] took into account four important flow parameters, namely the channel conditions, the packet delay, the flow queue size and the flow type, to compute the scheduling metric using the Jain's index for each flow before assigning each resource block (RB) to the flow of the highest metric. However, both [11] and [12] developed their scheduling algorithms by optimizing ratio-based metrics, following the traditional PFS design. Since such ratios do not have practical physical interpretations, these ratio-based algorithms cannot provide any guarantee on the actual data rate achieved by each user.

Inspired by the discussions above, we argue that rate-fairness is a more appropriate metric in designing scheduling algorithms for bursty traffic. In particular, we consider the 5%-tile user data rate (5TUDR), i.e., the 5% worst user data rate, to evaluate the user fairness. Unlike the time-fairness, the 5TUDR metric caters to inferior users without ignoring the overall network throughput. As a result, it is feasible to optimize the 5TUDR metric while implicitly maintaining a satisfactory average user data rate (AUDR). Indeed, the 5TUDR metric has been commonly employed to evaluate network performance by most wireless network operators in practice [4]. However, it is challenging to use 5TUDR in practical network design due to the following reasons. First, since AUDR is governed by factors across multiple network layers, it is technically infeasible to develop a mathematical model to optimize AUDR or 5TUDR. Furthermore, 5TUDR is a long-term performance metric over multiple TTIs after a sequence of resource allocation decisions. Thus, 5TUDR cannot be directly optimized by any single-step scheduling algorithms such as PFS. In particular, if we consider allocating multiple RBGs to multiple users, the optimization space grows exponentially with time, which makes the design problem analytically intractable.

To overcome these challenges, we propose to first cast the RBG allocation task as a cooperative game in which multiple RL agents collaboratively optimize a common objective function using the same reward function. After that, we devise a computationally efficient Multi-Agent Reinforcement Learning (MARL)-based scheduling algorithm to learn a dis-

tributed policy by decomposing the action space into multiple smaller action spaces. The main contributions of this paper are summarized as follows:

- We propose to model the RBG allocation process as a stochastic game by taking into account information from multiple network layers for both full-buffer and bursty downlink traffic. To maximize the user fairness without sacrificing the network throughput, we propose a novel reward function specifically designed to optimize 5TUDR;
- Based on the proposed stochastic game, we then develop a MARL-based algorithm to optimize the scheduling policy that achieves good 5TUDR performance while maintaining a considerable AUDR.
- Finally, extensive simulation is performed to validate the performance of the proposed MARL scheduler. The experiment results are analyzed in details to provide insights about the learned scheduling policy.

The remainder of the paper is organized as follows: Sec. II provides the system model and the problem formulation. Sec. III elaborates the framework of the stochastic game for RBG allocation. After that, Sec. IV proposes the MARL algorithm for solving the stochastic game. Finally, Sec. V shows the simulation results before Sec. VI concludes the paper.

II. SYSTEM MODEL AND PROBLEM FORMULATION

A. System Model

We consider a wireless network in which a base station (BS) schedules K RBGs to multiple active user equipments (UEs) in the downlink operating in the Frequency Division Duplexing (FDD) mode. The UE arrival is modeled as a random process following the Poisson distribution with an arrival rate of λ . Upon arrival, each UE requests a finite amount of traffic data from the BS. The BS divides its frequency resources into RBGs with each RBG being allocated to at most one UE in each TTI as shown in Fig. 1. Furthermore, if a user is scheduled, its requested data will be transferred to an HARQ buffer. For each transmitted package, the ACK/NACK message is fed back from the targeted UE at a fixed time interval. Upon receiving a NACK message, the BS will re-transmit the corresponding data package. A UE departs from the network immediately after all its requested data is successfully received, which effectively emulates the bursty traffic mode. In our work, some practical network mechanisms such as the Out Loop Link Adaptation (OLLA) are included in our model. More details about the network mechanisms considered in this work can be found in Appendix A.

B. Problem Formulation

We begin with the definitions of two key metrics employed in this work, namely AUDR and 5TUDR.

1) *Average User Data Rate (AUDR)*: Without loss of generality, we focus on the first T TTIs. We denote by t_a^n and t_d^n the TTI indices when the n -th user enters and exits the network, respectively, with $1 \leq t_a^n \leq t_d^n \leq T$. Furthermore,

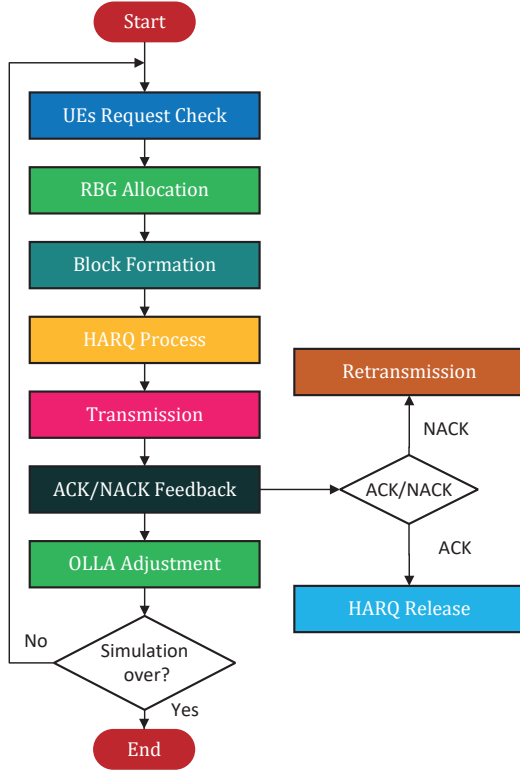


Fig. 1. Network Mechanisms

we denote by N_t the number of users who have arrived by the t -th TTI with $t \in [1, T]$. It should be emphasized that some of these N_t users may have left the network by the t -th TTI if they finish their transmissions earlier than the t -th TTI. Thus, we can express the corresponding AUDR over $[1, T]$ as:

$$D(t) = \frac{1}{N_t} \sum_{n=1}^{N_t} \psi^n(t), \quad (1)$$

where $\psi^n(t)$ is the user data rate (UDR) of the n -th user over $[t_a^n, t]$ takes the following form:

$$\psi^n(t) = \frac{\sum_{i=t_a^n}^t T^n[i] I^n[i]}{\min(t, t_d^n) - t_a^n}. \quad (2)$$

In Eq. (2), $T^n[i]$ is the packet size designated for the n -th user during the i -th TTI. Furthermore, $I^n[i]$ is the indicator function for the ACK/NACK feedback with “1” indicating a successful transmission while “0” a transmission failure. Note that the numerator in Eq. (2) stands for the total amount of successfully transmitted data while the denominator the time duration of the n -th user spent in the system.

2) **5%-Tile User Data Rate (5TUDR):** Next, we denote by ϕ_t the 5%-tile user data rate and have:

$$\phi_t = P_{5\%}(\mathcal{W}(t)), \quad (3)$$

where $P_{5\%}(\cdot)$ is the operator to find the 5%-tile element in the enclosed set and

$$\mathcal{W}(t) = \{\psi^1(t), \dots, \psi^{N_t}(t)\}. \quad (4)$$

Equipped with the two definitions above, we are ready to formulate our problem. Given a network described above, our goal is to establish an optimal scheduling policy denoted by π that maximizes the rate-fairness metric 5TUDR over the time interval $[1, T]$. Specifically, the optimization problem can be written as

$$\begin{aligned} \mathcal{P}_1 : \quad & \arg\max_{\pi} \phi_T(\pi) \\ \text{subject to} \quad & C_1 : D(T) \geq \kappa, \\ & C_2 : P(N_t) = \frac{\lambda^{N_t}}{N_t!} e^{-\lambda}, \quad \forall t \in [1, T] \end{aligned} \quad (5)$$

where κ in Constraint C_1 is the minimum required AUDR while C_2 defines that the probability of having N_t new arriving users follows the Poisson distribution with an average arrival rate of λ .

Clearly, it is non-trivial to find the optimal policy π^* by directly solving \mathcal{P}_1 as the optimization space grows exponentially with the number of active users, the number of RBGs under consideration as well as the time duration. In the sequel, we will first transform \mathcal{P}_1 into a stochastic game before a MARL-based scheduling algorithm is developed to exploit data from multiple network layers.

III. STOCHASTIC GAME FRAMEWORK FOR RBG ALLOCATION

Stochastic games can be considered as the generalization of the Markov Decision Process (MDP) with multiple agents. If all agents work together to maximize a collective return, then the stochastic game is called a cooperative game [13]. Fig. 2 illustrates the overview of this cooperative game for the task of RBG allocation.

In the following discussions, we will concentrate on the scheduling decision for the t -th TTI. For simplicity of presentation, we will ignore the time index in the notations in this section. In this game, we arrange K agents to allocate a set of K RBGs independently with each agent using an independent scheduling policy π_k whose output is the action u_k representing the allocation decision of the k -th agent. We denote by $\mathbf{u} = (u_1, \dots, u_K)$ the joint action of all K agents.

Definition 1. This cooperative game can be defined by a tuple $\mathcal{E} = \langle \mathcal{S}, \mathcal{U}, \mathcal{A}, P, r, \mathcal{Z}, \mathcal{O}, \gamma \rangle$ [14], where:

- \mathcal{Z} : the local observation space with $\mathbf{o}_k \in \mathcal{Z}$;
- \mathcal{S} : the global state space;
- \mathcal{U} : the action space for each agent;
- \mathcal{A} : the set of all agents indexed by $k = 1, 2, \dots, K$;
- $P(\mathbf{s}' | \mathbf{s}, \mathbf{u})$ of $\mathcal{S} \times \mathcal{U} \times \mathcal{S} \rightarrow [0, 1]$: the transition probability, where $\mathbf{s}, \mathbf{s}' \in \mathcal{S}$ and $\mathbf{u} \in \mathcal{U} \equiv \mathcal{U}^{|\mathcal{A}|}$;
- $r(\mathbf{s}, \mathbf{u})$ of $\mathcal{S} \times \mathcal{U} \rightarrow \mathbb{R}$: the reward function that evaluates the reward for a given state-action pair;
- $\mathcal{O}(\mathbf{s}, k)$: $\mathcal{S} \times \mathcal{A} \rightarrow \mathcal{Z}$: the observation function;

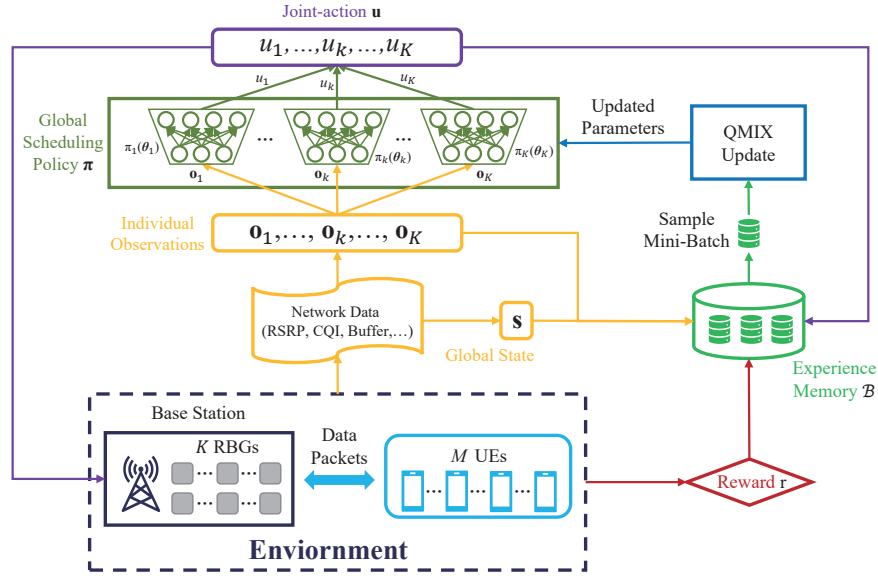


Fig. 2. The overview of the cooperative game of the RBG allocation.

- $\gamma \in [0, 1]$ is a discount factor.

At each TTI, each of the K agents first observes the environment and gathers network data to form its local observation o_k before choosing its action. It should be emphasized that we propose not to use the global state s that is the collection of all local observations $\{o_k\}$ in this decision-making stage. Instead, s will be used to update the scheduling policy in Sec. IV. Upon receiving the decisions, the BS performs the corresponding transmission as specified by the agents. After that, the reward function will generate a total reward for all agents to evaluate the overall allocation performance. Finally, the observations, actions and rewards will be stored in the experience memory for the scheduling policy update. The details about the policy update will be elaborated in Sec. IV. In the following, we propose the states, the actions and the reward function employed in the cooperative RBG allocation game.

A. Cross-layer Observation and Adaptive Action

For a traditional model-based scheduler, it can only utilize information from one single network layer due to the prohibitively high complexity incurred in modeling information from multiple layers. In this paper, we propose to better characterize the network status by exploiting information from multiple network layers.

TABLE I
NETWORK DATA OF OBSERVATIONS

Counter Name	Layer	Dimension
RSRP	PHY	1
Average of RB CQI	PHY	1
Buffer size	MAC	1
Scheduled frequency	MAC	1
OLLA offset	MAC	1
Historical user data rate (HURD)	MAC	1

Table I shows the network counters selected in our design as well as the layer that each counter belongs to. For instance, Reference Signal Receiving Power (RSRP) is selected to represent the longer-term wireless signal strength while Channel Quality Indicator (CQI) is employed to reflect the instantaneous channel quality corresponding to the channel's signal-to-noise ratio (SNR). Note that the CQI value for the same user varies in different RBGs due to the frequency-selective channels commonly encountered by the broadband wireless communication systems. Furthermore, we take into account the buffer size that stands for the amount of remaining data to be transferred to an active user as well as each user's scheduled frequency that keeps track of how often each user has been scheduled for transmission. Finally, the historical user data rate (HURD) and the OLLA offset are also included in our observations. As indicated in Table I, all these network parameters are taken from either the physical (PHY) or the multiple access (MAC) layers. It should be emphasized that more counters can be included in our observation in a straightforward manner at the cost of higher computational complexity.

At each TTI, each agent forms its observation based on the counters listed in Table I. We denote by C and M the total number of network counters under consideration and the

number of active users at the current TTI, respectively. We can then construct an $M \times C$ feature matrix \mathbf{O} based on the individual observation from each agent as follows:

$$\mathbf{O}_k = \begin{pmatrix} f_k^{1,1} & \cdots & f_k^{1,C} \\ \vdots & \ddots & \vdots \\ f_k^{M,1} & \cdots & f_k^{M,C} \end{pmatrix}, \quad (6)$$

where $f_k^{m,c}$ stands for the c -th counter value over the k -th RBG observed by the m -th user with $m = 1, 2, \dots, M$ and $c = 1, 2, \dots, C$. For instance, assuming that CQI is labeled as the first counter, then $f_k^{m,1}$ represents the CQI of the m -th user over the k -th RBG. However, for *bursty traffic*, the dimension of this feature matrix \mathbf{O}_k varies with M over time, which makes the problem very challenging for the agents to allocate a fixed number of RBGs to an uncertain number of users.

To circumvent this problem, we propose to apply the following operation on \mathbf{O}_k :

$$\mathbf{o}_k = \text{Vec}(\mathbf{O}_k^T \mathbf{O}_k), \quad (7)$$

where the operator $\text{Vec}(\cdot)$ converts the enclosed matrix into a single vector row by row. Note that the resulting vector \mathbf{o}_k has a fixed length of C^2 where C is the total number of network counters included in our observation.

Capitalizing on \mathbf{o}_k of a fixed length, we propose to employ deep neural networks (DNNs) to characterize the individual scheduling policy [15]. More specifically, we denote by $\pi_k(\boldsymbol{\theta}_k)$ the k -th agent's individual scheduling policy parameterized by a DNN of parameters $\boldsymbol{\theta}_k$. Each agent first generate priority values to all active users based on $\pi_k(\boldsymbol{\theta}_k)$ before assigning its RBG to the best user. However, the number of active users varies with time if bursty traffic is considered. To cope with this problem, we propose to pre-define a maximum number of active users denoted by M_{\max} . As a result, the output layer of the DNN parameterized by $\boldsymbol{\theta}_k$ has a constant dimension of M_{\max} among which M users are the actual active users and $M_{\max} - M$ virtual users.

B. Reward Function

To harvest the benefit of being able to accurately characterize the network status stated above, we will next devise a well-defined reward function to evaluate the performance of each agent. Since the design goal is to maximize 5TUDR while maintaining a considerable AUDR, the desired reward function should be able to evaluate the contribution of each scheduling decision towards the final 5TUDR and AUDR. A trivial 5TUDR-maximizing reward function can be designed to maximize the increment in 5TUDR between two consecutive TTIs. Unfortunately, the performance of such reward functions has been found very poor with bursty traffic. Fig. 3 shows the increment of 5TUDR as a function of time in TTI. Inspection of Fig. 3 reveals that the increment of 5TUDR is always 0 with occasional sharp increases and decreases. Careful investigation on those sharp spikes indicates that those sharp decreases were caused by the arrival of new users whose ϕ_t is 0. In

contrast, once this new user was scheduled, its user data rate suddenly became non-zero, which caused a sharp increase in the increment of 5TUDR. Therefore, using the increment of 5TUDR as the reward function is not appropriate for bursty traffic as the increment is a random event due to the arrival or departure of users.

Alternatively, we can consider employing the increment of AUDR as the reward function. However, the increment of AUDR is also heavily influenced by the arrival or departure of users. Fig. 4 illustrates an example of the increment of AUDR between two consecutive TTIs. In Fig. 4, the sharp decreases of AUDR were caused by the arrival of new users as their contribution of zero data rates to AUDR. In contrast, the sharp increases occurred when the agents allocated RBGs to users of advantageous channel conditions and large data packets were transmitted in a short period of time. Clearly, the increment of AUDR is not an appropriate reward function to maximize 5TUDR either.

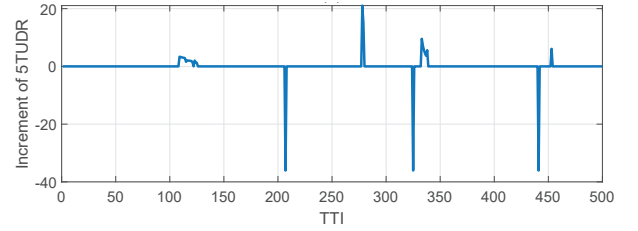


Fig. 3. An example of the increment (decrement when negative) of 5TUDR between two consecutive TTIs over time.

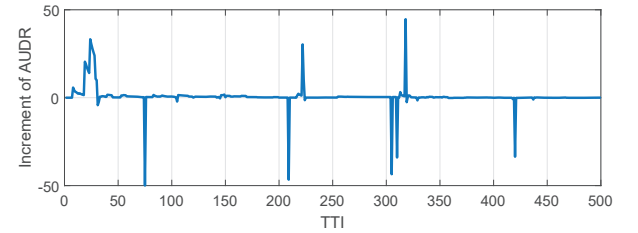


Fig. 4. An example of the increment (decrement when negative) of AUDR between two consecutive TTIs over time.

To strike the balance between 5TUDR and AUDR, we propose the following reward function by exploiting the changes of the *sum* of AUDR and the *sum* of UDR over two consecutive TTI's, respectively.

$$r(t) = h \left(\sum_{n=1}^{N_t} \psi^n(t) - \sum_{n=1}^{N_{t-1}} \psi^n(t-1) \right) - \exp\{-\mathcal{G}(\Delta\Psi(t))\}, \quad (8)$$

where $h(\cdot)$ is the sigmoid function and $\Delta\Psi(t)$ stands for the UDR change of each user given by

$$\Delta\Psi(t) = (\Delta\psi^1(t), \dots, \Delta\psi^{N_t}(t)), \quad (9)$$

with $\Delta\psi_t^n = \psi^n(t) - \psi^n(t-1)$ for $n = 1, 2, \dots, N_t$. In addition, $\mathcal{G}(\cdot) \in [0, 1]$ is the G's fairness index that measures

the level of variations of the elements of the enclosed vector [16].

It is worth mentioning the following features of the proposed reward function in Eq. (8). First, the reward function is conditioned upon the sum of all user data rates, which makes the reward function insensitive to the time-varying number of total arrived users. In particular, when new users of zero UDR enter the system, the reward function is not affected. Second, since the reward function effectively maximizes the increment in the user data sum-rate, the resulting scheduling policy drives all agents to effectively allocate RBGs. Finally, the G's fairness index is introduced as the regularization term to discourage agents to be in favor of a few users. As a result, more users will be given transmission opportunities, which effectively improves 5TUDR.

With the proposed reward function, we are ready to convert the optimization problem in Eq. (5) as follows:

$$\begin{aligned} \mathcal{P}_2 : \quad & \underset{\pi}{\operatorname{argmax}} \mathbb{E} \left[\sum_{t=1}^T \gamma^t r(t) | \pi \right] \\ \text{subject to} \quad & C_1 : D(T) \geq \kappa \\ & C_2 : P(N_t) = \frac{\lambda^{N_t}}{N_t!} e^{-\lambda} \quad \forall t \in [1, T] \end{aligned} \quad (10)$$

where the expectation is taken over the randomness of the allocation trajectories. In particular, Eq. (10) indicates that the objective of this cooperative game is to find a policy π that maximizes the long-term return. All agents are allowed to explore diverse policies as long as Eq. (10) is maximized. For such a cooperative game problem, the Nash Equilibrium (NE) is commonly employed to describe the solution [17]. Unfortunately, it is non-trivial to find NE in many practical scenarios. To cope with this problem, a learning algorithm based on the Multi-Agent Reinforcement Learning (MARL) is proposed in the next section.

IV. MARL-BASED ALGORITHM

In this section, we will first review some basics about MARL before introducing a popular MARL algorithm called QMIX.

A. MARL Background

MARL learns from the interactions with the environment and subsequently, updates its policy to maximize the long-term return. To evaluate the policy, the action-value function is leveraged to characterize the expected return. More specifically, the expected return takes the following form if the agents execute the joint-policy π after taking joint-action \mathbf{u} at the global state \mathbf{s} :

$$Q^\pi(\mathbf{s}, \mathbf{u}) = \mathbb{E}_\pi \left[\sum_{t=0}^{\infty} \gamma^t r_t | \mathbf{s}_0 = \mathbf{s}, \mathbf{u}_0 = \mathbf{u} \right] \quad (11)$$

The action-value function between two consecutive state-action pairs $(\mathbf{s}', \mathbf{u}')$ and (\mathbf{s}, \mathbf{u}) satisfies the Bellman Equation [19]:

$$Q^\pi(\mathbf{s}, \mathbf{u}) = \mathbb{E}_{\pi, P} [r(\mathbf{s}, \mathbf{u}) + \gamma Q^\pi(\mathbf{s}', \mathbf{u}')] \quad (12)$$

Moreover, the Bellman Optimal Theorem indicates that the optimal policy π^* satisfies:

$$Q^{\pi^*}(\mathbf{s}, \mathbf{u}) = \sup_{\pi \in \Pi} \{Q^\pi(\mathbf{s}, \mathbf{u})\}, \quad (13)$$

where Π is the set of stationary policies.

By exploiting Eq. (12) and Eq. (13), the Bellman Optimality Equation can be found as:

$$Q^*(\mathbf{s}, \mathbf{u}) = \mathbb{E}_{\pi^*, P} \left[r(\mathbf{s}, \mathbf{u}) + \gamma \max_{\mathbf{u}' \in \mathcal{U}} \{Q^*(\mathbf{s}', \mathbf{u}')\} \right] \quad (14)$$

Finally, we define the Bellman optimality operator \mathcal{T}^* as:

$$\mathcal{T}^*(Q^\pi(\mathbf{s}, \mathbf{u})) = \mathbb{E}_{\pi, P} \left[r(\mathbf{s}, \mathbf{u}) + \gamma \max_{\mathbf{u}' \in \mathcal{U}} \{Q^\pi(\mathbf{s}', \mathbf{u}')\} \right] \quad (15)$$

It has been proved that iterative updates of $Q^\pi(\mathbf{s}, \mathbf{u})$ with $\mathcal{T}^*(Q^\pi)$ lead to its convergence towards $Q^{\pi^*}(\mathbf{s}, \mathbf{u})$ [20]. To overcome the high-dimensional state space, it is a common technique to use the function approximation to represent the action values. Denote by $Q_\sigma^\pi(\mathbf{s}, \mathbf{u})$ the action-value function parameterized by a DNN with parameters σ , the optimization objective can be transformed to find σ with $Q_\sigma^\pi(\mathbf{s}, \mathbf{u})$. The optimal parameters σ can be derived by minimizing the following temporal difference error [21]:

$$\mathcal{L}(\sigma) = \left[r(\mathbf{s}, \mathbf{u}) + \gamma \max_{\mathbf{u}' \in \mathcal{U}} \{Q_\sigma^\pi(\mathbf{s}', \mathbf{u}')\} - Q_\sigma^\pi(\mathbf{s}, \mathbf{u}) \right]^2 \quad (16)$$

B. QMIX

In the multi-agent learning problem, it is not straightforward to learn the action-value function $Q_\sigma^\pi(\mathbf{s}, \mathbf{u})$ due to the exponentially growing dimension of the joint-action space. To address this problem, the QMIX algorithm was developed to learn the joint-action value function through value decomposition [22]. QMIX is a model-free, value-based, off-policy, decentralized execution but centralized training algorithm designed for cooperative tasks. QMIX employs the DNN-based function approximation approach to estimate the action-value function [22].

Fig. 5 illustrates the architecture of QMIX. Implemented in decentralized control systems, QMIX allows each agent k to maintain an individual action-value function $Q_k(\mathbf{o}_k, u_k)$ that is conditioned upon each individual observation \mathbf{o}_k and local action u_k . In every step, each agent k accepts an individual observation \mathbf{o}_k and generates the corresponding action values. After that, the action is determined using the ϵ -greedy principle with the probability of choosing the action u_k given by [23]:

$$P(u_k | \mathbf{o}_k) = \begin{cases} 1 - \epsilon + \frac{\epsilon}{|\mathcal{U}|}, & u_k = \underset{u_k}{\operatorname{argmax}} \{Q_k(\mathbf{o}_k, u_k)\} \\ \frac{\epsilon}{|\mathcal{U}|}, & u_k \neq \underset{u_k}{\operatorname{argmax}} \{Q_k(\mathbf{o}_k, u_k)\} \end{cases}, \quad (17)$$

where $|\mathcal{U}|$ is the cardinality of the action space.

This policy requires each agent to randomly select an action from the action space with a probability of ϵ , or follow the action with the maximum action-value with a probability of $1 - \epsilon$. This policy encourages abundant explorations by

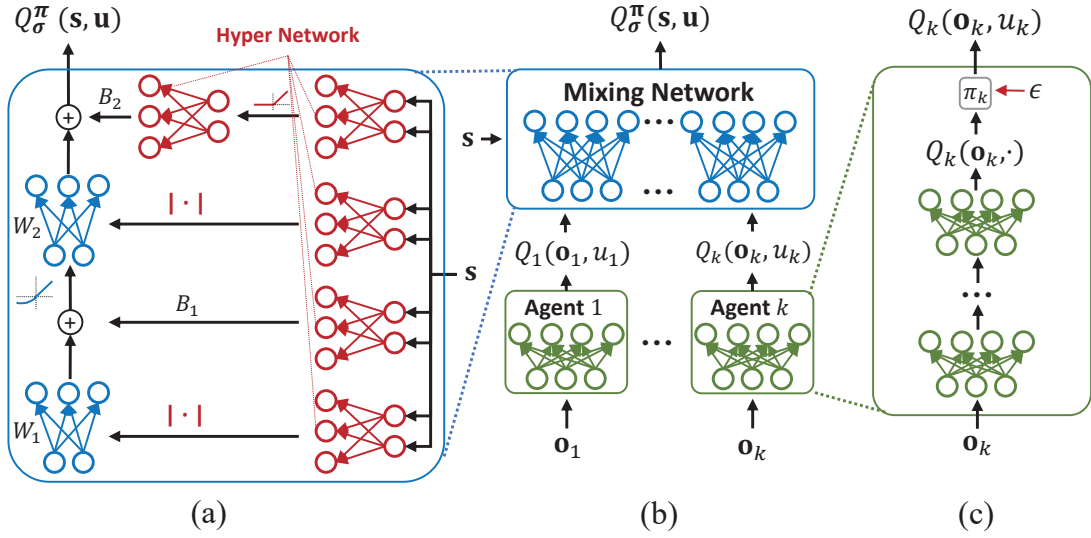


Fig. 5. (a) Mixing network structure. In red are the hypernetworks that produce the weights and biases for mixing network layers shown in blue. (b) The overall QMIX architecture. (c) Agent network structure. (d) The GRU structure, where h is the hidden information used for recursion [18].

assigning non-zero probability to explore all possible state-action pairs during training. To guarantee the consistency between Q_σ^π and Q_k , QMIX ensures that the global argmax operation applied on the centralized $Q_\sigma^\pi(s, u)$ generates the same result as a set of argmax operation applied on each Q_k :

$$\arg\max_u \{Q_\sigma^\pi(s, u)\} = \begin{pmatrix} \arg\max_{u_1} \{Q_1(o_1, u_1)\} \\ \vdots \\ \arg\max_{u_k} \{Q_k(o_k, u_k)\} \end{pmatrix} \quad (18)$$

Mathematically, this imposes a monotonicity constraint on the relationship between $Q_\sigma^\pi(s, u)$ and each Q_k :

$$\frac{\partial Q_\sigma^\pi(s, u)}{\partial Q_k} \geq 0, \forall k. \quad (19)$$

If the centralized training is performed, QMIX leverages a mixing network to calculate the centralized action-value function. The mixing network consists of two parts, the backbone and hyper-networks. Let \mathcal{H}_δ and \mathcal{M}_σ denote the hyper-network and the mixing network parameterized by parameters δ and σ , respectively. At the t -th TTI, the hyper-network accepts the global state s_t and generates weights and biases for the mixing network:

$$\sigma_t = \mathcal{H}_\delta(s_t) \quad (20)$$

Moreover, all the generated weights are set to be positive to satisfy Eq. (19). With reference to Fig. 5, we denote by W_1, W_2, B_1 and B_2 the generated weights and biases from the hyper-network, respectively. Furthermore, $\mathbf{Q} = (Q_1, \dots, Q_K)$ stands for the input vector of the individual action-values, then $Q_\sigma^\pi(s, u)$ can be written as:

$$\begin{aligned} Q_\sigma^\pi(s, u) &= W_2 \cdot g(W_1 \mathbf{Q} + B_1) + B_2, \\ &= W_2 \cdot g(Y_1) + B_2, \end{aligned} \quad (21)$$

where

$$g(x) = \begin{cases} \alpha(e^x - 1) & x < 0, \alpha > 0 \\ x, & x \geq 0 \end{cases} \quad (22)$$

is the standard ELU activation function.

Taking the derivative with respect to \mathbf{Q} on both sides of Eq. (21) using the chain rule, we have

$$\begin{aligned} \frac{\partial Q_\sigma^\pi(s, u)}{\partial \mathbf{Q}} &= \frac{\partial Q_\sigma^\pi(s, u)}{\partial g(Y_1)} \cdot \frac{\partial g(Y_1)}{\partial Y_1} \cdot \frac{\partial Y_1}{\partial \mathbf{Q}}, \\ &= W_2 \cdot g'(W_1 \mathbf{Q} + B_1) \cdot W_1. \end{aligned} \quad (23)$$

Recalling Eq. (22), we have

$$g'(x) = \begin{cases} \alpha e^x & x < 0, \alpha > 0 \\ 1 & x \geq 0 \end{cases} \quad (24)$$

Since W_1 and W_2 are non-negative, we can show that

$$\frac{\partial Q_\sigma^\pi(s, u)}{\partial Q_k} \geq 0, \forall k. \quad (25)$$

Thus, the global state is integrated into the centralized action-value function by the hyper-network. Finally, QMIX is trained by minimizing the following loss function:

$$\mathcal{L}(\theta, \delta, \sigma) = [r + \gamma \max_{u'} Q_\sigma^\pi(s', u') - Q_\sigma^\pi(s, u)]^2, \quad (26)$$

where θ contains the DNN parameters of all agents. Note that Eq. (26) takes the similar form as Eq. (16) for the update operations. Finally, the QMIX-based algorithm updates the scheduling policy as summarized in Algorithm 1.

V. SIMULATION AND ANALYSIS

In this section, we will perform extensive computer simulation using the network simulator defined in Section II. The simulated network includes many practical network mechanisms as shown in Appendix A. Table II summarizes the parameters employed in the simulation.

Algorithm 1 The QMIX algorithm for User Scheduling

- 1: Initialize K agent networks $\{Q_{\theta_1}, \dots, Q_{\theta_K}\}$ with DNN parameters $\theta = \{\theta_1, \dots, \theta_K\}$;
- 2: Initialize the hyper-network \mathcal{H}_δ and the mixing network \mathcal{M}_σ with parameters δ and σ ;
- 3: Set a replay buffer \mathcal{B} , learning rate λ , discount factor γ and ϵ ;
- 4: **for** $t = 1, \dots, T$ **do**
- 5: Each agent k makes its local action $u_k(t)$ based on its local observation $\mathbf{o}_k(t)$ using the ϵ -greedy policy before observing a new local state $\mathbf{o}_k(t+1)$;
- 6: Execute the joint-action $\mathbf{u}(t)$ and evaluate the total reward $r(t)$ before collecting the new global state $\mathbf{s}(t+1)$;
- 7: Store the following transition in \mathcal{B} for $k \in \{1, \dots, K\}$:

$$(\mathbf{s}(t), r(t), \mathbf{s}(t+1)), (\mathbf{o}_k(t), \mathbf{o}_k(t+1), u_k(t))$$
- 8: Sample a random mini-batch of b transitions from \mathcal{B} :

$$(\mathbf{s}(i), r(i), \mathbf{s}(i+1)), (\mathbf{o}_k(i), \mathbf{o}_k(i+1), u_k(i)), \forall k$$
- 9: Derive K individual Q values:

$$\mathbf{Q} = (Q_{\theta_1}(\mathbf{o}_1(i), u_1(i)), \dots, Q_{\theta_K}(\mathbf{o}_K(i), u_K(i)))$$

$$\mathbf{Q}' = (Q_{\theta_1}(\mathbf{o}_1(i+1), u_1(i+1)), \dots, Q_{\theta_K}(\mathbf{o}_K(i+1), u_K(i+1)))$$
- 10: Calculate weights for mixing network, then get $Q_\sigma^\pi(\mathbf{s}(i), \mathbf{u}(i))$ and $Q_\sigma^\pi(\mathbf{s}(i+1), \mathbf{u}(i+1))$:

$$\sigma(i) \leftarrow \mathcal{H}_\delta(\mathbf{s}(i)),$$

$$\sigma(i+1) \leftarrow \mathcal{H}_\delta(\mathbf{s}(i+1))$$

$$Q_\sigma^\pi(\mathbf{s}(i), \mathbf{u}(i)) \leftarrow \mathcal{M}_{\sigma(i)}(\mathbf{Q})$$

$$Q_\sigma^\pi(\mathbf{s}(i+1), \mathbf{u}(i+1)) \leftarrow \mathcal{M}_{\sigma(i+1)}(\mathbf{Q}')$$
- 11: Set $y(i) = r(i) + \gamma \max_{\mathbf{u}(i+1)} \{Q_\sigma^\pi(\mathbf{s}(i+1), \mathbf{u}(i+1))\}$
- 12: Update all the agent networks and hyper-network by minimizing the following loss:

$$\mathcal{L}(\theta, \sigma, \delta) = \sum_{i=1}^b \left[(y(i) - Q_\sigma^\pi(\mathbf{s}(i), \mathbf{u}(i)))^2 \right]$$

13: **end for**

TABLE II
BS PARAMETERS USED IN SIMULATION

Parameters	Values
Transmit power for each RB	18 dBm
Number of RB for each RBG	3
Number of RBGs	3
Frequency bandwidth for each RBG	10MHz
Noise power density	-174 dBm/Hz
Minimum MCS	1
Maximum MCS	29
Maximum number of HARQ	8
Feedback period of HARQ	8
Initial RB CQI value	4

For illustration purposes, only three RBGs are deployed in the BS with each RBG composed of three RBs. In particular, each HARQ process can have at most eight re-transmissions with the ACK/NACK message is returned with a delay of seven TTIs.

A. Model Training

The agents are trained using the parameters listed in Table III. Each epoch represents one scheduling process of 1000 TTIs. In each epoch, BS will continue to accept new users while all agents perform RBG allocation until the end of the epoch. This process is designed to produce the experience data composed of the state-action pairs and the corresponding rewards. After that, each agent will select a mini-batch of experience data to update its parameters. The batches and the batch size are set to 10 and 256, respectively.

TABLE III
PARAMETERS FOR TRAINING.

Parameters	Values
Epoch	100
Duration of one experiment	1000 TTIs
Learning rate	1e-3
Learning rate decay	1e-7
Batches	10
Batch size	256
Replayer capacity	2000
ϵ	1e-2
Initial number of users	5
Average of Poisson distribution (λ)	1e-2

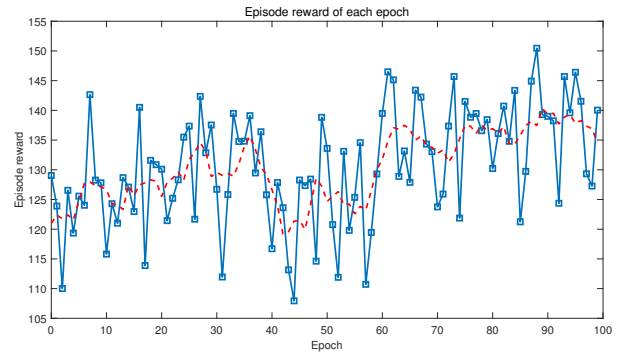


Fig. 6. Episode reward as a function of epochs.

As shown in Fig. 6, the episode reward increased with the training epoch throughout the training process.

B. Performance Comparison

Next, we compare the performance of the proposed scheduler against the conventional OPS, RRS and GPFS. Since the performance of GPFS is influenced by its two parameters, namely α_1 and α_2 , we will first investigate the appropriate α_1 values to optimize the resulting 5TUDR performance using computer simulation.

Fig. 7 shows the 5TUDR performance averaged over 1000 experiments as a function of α_1 for GPFS, RRS and OPS.

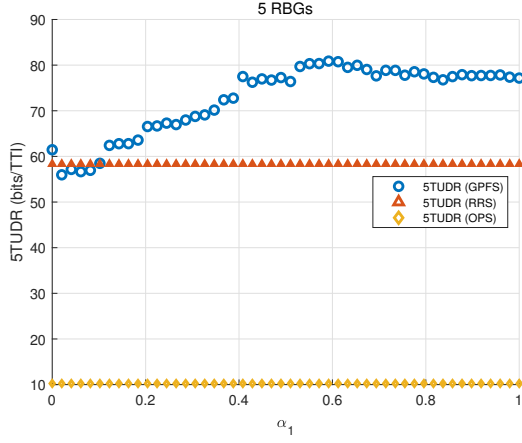


Fig. 7. The 5TUDR performance as a function of α_1 .

Inspection of Fig. 7 reveals that the 5TUDR performance of GPFS initially increases with α_1 before it saturates after $\alpha_1 = 0.5$. This is because a larger α_1 encourages GPFS to give higher scheduling priorities to users of better channel conditions, which initially improves both the AUDR and 5TUDR performance by more efficiently utilizing the network resources. However, any further increase in α_1 deteriorated the data rates of the users of poor channel conditions, which became detrimental to the 5TUDR performance of the network. In contrast, the performance of RRS and OPS is independent of α_1 that is not a parameter in RRS and OPS. It is evidenced from Fig. 7 that OPS had the worst 5TUDR performance while GPFS with $\alpha_1 = 0.5$ outperformed OPS and RRS in terms of 5TUDR. In the sequel, we define GPFS1 as GPFS with $\alpha_1 = 0$ and $\alpha_2 = 1$ while GPFS2 as GPFS with $\alpha_1 = 0.5$ and $\alpha_2 = 1$.

Next, we will compare the AUDR and 5TUDR performance of the proposed MARL-based scheduler against GPFS1, GPFS2 and RRS. More specifically, we compute the improvement of the proposed scheduler over the four aforementioned conventional schedulers using 100 experiments. Fig. 8 and Fig. 9 plot the cumulative distribution function (CDF) of the improvements in terms of AUDR and 5TUDR, respectively. A positive x-axis value indicates that the proposed scheduler outperforms the conventional scheduler in comparison. As shown in Fig. 8, the proposed scheduler substantially outperformed GPFS2 and RRS in terms of AUDR while suffering from marginal AUDR degradation as compared to GPFS1 that is optimized for AUDR as shown in Fig. 7. More specifically, the average AUDR improvement achieved by the proposed MARL-based scheduler was 83.20 Bits/TTI and 147 Bits/TTI as compared to GPFS1 and RRS, respectively while the average AUDR degradation as compared to GPFS2 was 29.84 Bits/TTI. Furthermore, Fig. 9 shows the CDF of the 5TUDR improvement. Clearly, the proposed scheduler significantly outperformed all three conventional schedulers in terms of 5TUDR, which is evidenced by the fact that most x-axis values are positive. Specifically, the proposed scheduler achieved an average 5TUDR improvement of 54.70 Bit/TTI,

39.42 Bits/TTI and 46.96 Bits/TTI as compared with GPFS1, GPFS2 and RRS, respectively. Based on the discussions above, we can see that the proposed MARL-based scheduler is able to achieve substantially better 5TUDR performance (i.e. higher fairness) while maintaining a considerably large AUDR.

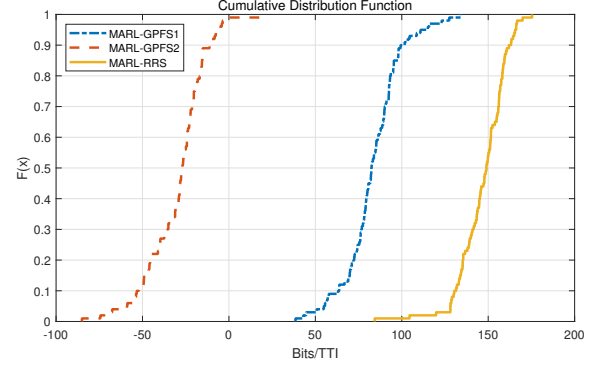


Fig. 8. CDF of the AUDR improvement achieved by the proposed algorithm as compared to PFS and RRS.

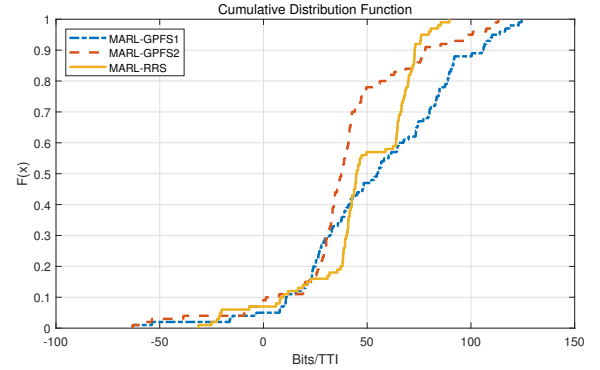


Fig. 9. CDF of the 5TUDR improvement achieved by the proposed algorithm as compared to PFS and RRS.

C. Analysis of the Learned Policy

To shed light on the policy learned by the proposed MARL-based scheduler, we will compare the scheduling preference of the proposed scheduler, GPFS1, GPFS2 and RFF. In the following simulation, we consider five users competing for three RBGs for bursty traffic over 500 TTIs.

1) More Transmission Time and Shorter Residence Time:

We will first investigate two metrics, namely the total transmission time and the total residence time of each user in the system. The transmission time of a user counts the number of TTIs that the user is allocated with RBGs for transmission. For instance, if three RBGs are allocated to three different users in one TTI, then the transmission time is counted as three. In contrast, if all three RBGs are allocated to the same user in one TTI, then the corresponding transmission time becomes one. In other words, the transmission time is designed to measure how often users are served over a period of time. Furthermore, the residence time is defined as the number of TTIs that

a user stays in the network before it completes its bursty transmission and leaves the network. Note that the residence time includes the time that a user spends on waiting for RBG allocation. We compare the total transmission time and the total residence time over all users for different schedulers in Fig. 10. Inspection of Fig. 10 suggests that the proposed MARL-based scheduler resulted in significantly reduced total residence time, which indicates that the proposed scheduler can finish the requested transmissions for all users within a much shorter time period by more efficiently utilizing the same network resources. Furthermore, the total transmission time over all users was significantly increased, which implies that the proposed scheduler tends to divide the available RBGs to different users and subsequently, all users were scheduled more frequently. This also explains the shorter residence time of all users as all users had more opportunities for being served. The results shown in Fig. 10 support our observation that the proposed scheduler resulted in higher AUDR and 5TUDR performance.

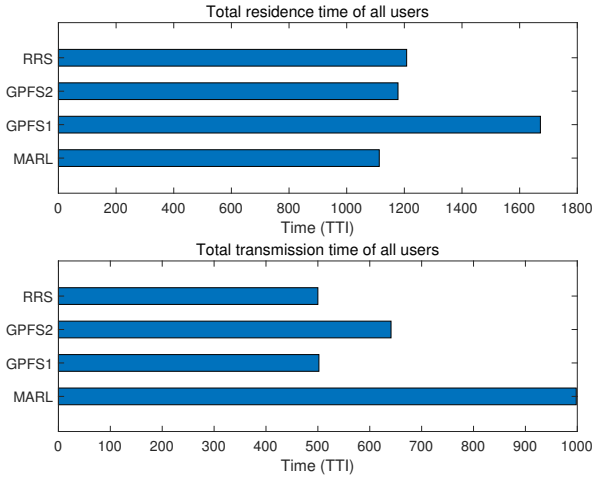


Fig. 10. Total residence time and total transmission time over all users.

2) *Diverse RBG Allocation:* As suggested in Fig. 10, the proposed MARL-based scheduler prefers allocating RBGs to diverse users, in lieu of concentrating all RBGs to only a few users. In this section, we will use data from two specific TTIs in a specific experiment to illustrate the different behaviors of the schedulers under consideration. Table IV and Table V document the RBG allocation results in TTI=1 and TTI=100, respectively. In Table IV, the first section details the counter information for each user. For the next four sections, we compare how each scheduler allocated each RBG. In particular, we use “T” and “F” to represent if the corresponding RBG was allocated or not allocated to the user indicated by the column index. For instance, the proposed scheduler allocated “RBG#2” to “UE#1” while “RBG#1” and “RBG#3” to “UE#4” who has better RSRP and a smaller data package for transmission indicated by the “Buffer” counter. In contrast, the three conventional schedulers allocated all RBGs to the

same user as all users have the identical CQI value across all RBGs.

TABLE IV
ALLOCATION EXAMPLE 1 (TTI=1)

	Attr.	UE#1	UE#2	UE#3	UE#4	UE#5
	RSRP	-99	-90	-96	-88	-70
	Buffer	94768	96288	15528	4400	36400
	HUUR	0.0	0.0	0.0	0.0	0.0
	CQI#1	4	4	4	4	4
	CQI#2	4	4	4	4	4
	CQI#3	4	4	4	4	4
MARL	RBG#1	F	F	F	T	F
	RBG#2	T	F	F	F	F
	RBG#3	F	F	F	T	F
GPFS1	RBG#1	T	F	F	F	F
	RBG#2	T	F	F	F	F
	RBG#3	T	F	F	F	F
GPFS2	RBG#1	T	F	F	F	F
	RBG#2	T	F	F	F	F
	RBG#3	T	F	F	F	F
RRS	RBG#1	T	F	F	F	F
	RBG#2	T	F	F	F	F
	RBG#3	T	F	F	F	F

After the network ran for 100 TTIs, we investigated the network counter information as well as the scheduling results in Table V. For the proposed scheduler, “UE#3”, “UE#4” and “UE#5” have already finished their transmission and left the network, which is indicated by “N/A” in Table V. As a result, only “UE#1” and “UE#2” were allocated RBGs. Despite the fact that “UE#2” had better channel conditions (indicated by its CQI and RSRP values) and a lower HUUR, the proposed scheduler was actually in favor of “UE#1”. This scheduling decision could be explained by the fact that “UE#1” has a smaller buffer size and may be able to finish its transmission in a shorter time. In contrast, GPFS2 and RRS only finished the transmission for “UE#4” and “UE#5” by TTI=100 while GPFS1 had four users remaining in the network. Note that GPFS1 and GPFS2 allocated more RBGs to “UE#1” as “UE#1” has the lowest HUUR among all remaining users.

Finally, we analyze the number of RBGs that each scheduler allocates to a single user in the same TTI. Fig. 11 shows the percentages of TTIs when a single user was allocated with “One”, “Two” or “Three” RBGs in the same TTI, recalling that our simulation only considered three RBGs. As indicated in Fig. 11, GPFS1 and RRS allocated all the RBGs to a single user almost throughout the entire simulation. In contrast, the proposed scheduler and GPFS2 chose to distribute their RBGs to different users more evenly. As a result, users are given more opportunities to access RBGs, which led to higher user fairness. In particular, the proposed scheduler never allocated all three RBGs to one single user, which makes our proposed scheduler very distinctive from the three conventional schedulers.

TABLE V
ALLOCATION EXAMPLE 2 (TTI=100)

	Attr.	UE#1	UE#2	UE#3	UE#4	UE#5
MARL	RSRP	-99	-90	N/A	N/A	N/A
	Buffer	86119	89886	N/A	N/A	N/A
	HUDR	72.1	42.9	N/A	N/A	N/A
	CQI#1	7	9	N/A	N/A	N/A
	CQI#2	7	9	N/A	N/A	N/A
	CQI#3	3	14	N/A	N/A	N/A
	RBG#1	T	F	F	F	F
	RBG#2	T	F	F	F	F
	RBG#3	F	T	F	F	F
GPFS1	RSRP	-99	-90	-96	N/A	-70
	Buffer	84563	87882	5360	N/A	2433
	HUDR	82.8	158.6	139.3	N/A	849.2
	CQI#1	7	9	7	N/A	25
	CQI#2	7	9	7	N/A	25
	CQI#3	3	14	9	N/A	27
	RBG#1	T	F	F	F	F
	RBG#2	T	F	F	F	F
	RBG#3	T	F	F	F	F
GPFS2	RSRP	-99	-90	-96	N/A	N/A
	Buffer	84663	86246	5884	N/A	N/A
	HUDR	81.6	182.3	132.1	N/A	N/A
	CQI#1	7	9	7	N/A	N/A
	CQI#2	7	9	7	N/A	N/A
	CQI#3	3	14	9	N/A	N/A
	RBG#1	T	F	F	F	F
	RBG#2	T	F	F	F	F
	RBG#3	F	T	F	F	F
RRS	RSRP	-99	-90	-96	N/A	N/A
	Buffer	88587	82716	5828	N/A	N/A
	HUDR	55.9	125.3	90.3	N/A	N/A
	CQI#1	7	9	7	N/A	N/A
	CQI#2	7	9	7	N/A	N/A
	CQI#3	3	14	9	N/A	N/A
	RBG#1	T	F	F	F	F
	RBG#2	T	F	F	F	F
	RBG#3	T	F	F	F	F

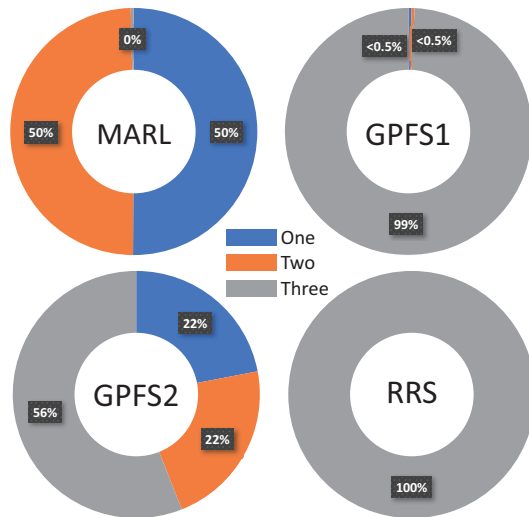


Fig. 11. Percentages of TTIs when a single user was allocated with “One”, “Two” or “Three” RBGs.

3) *Scheduling Preference*: Finally, we explore the scheduling preference of the proposed MARL-based scheduler. Unfortunately, the policy of the proposed scheduler is represented by a set of DNN parameters, which makes the analysis challenging. To cope with this challenge, we first analyze the scheduling log data as shown in Table IV and Table V. Specifically, “UE#1” and “UE#2” in Table IV and Table V had a much larger buffer size than the other three users. By TTI=100, the proposed scheduler has completed the data transmission for those users of a smaller buffer size without holding these users waiting in the network. As a result, the average user data rates for those users were improved, which in turns contributed to the increase in AUDR. Therefore, it is reasonable to conjecture that the proposed scheduler prefers scheduling the users of a smaller buffer size first. To validate this conjecture, we first investigate the number of active users waiting for services in each TTI by different schedulers. Fig. 12 shows that the number of active users in the network was reduced from 5 to 2 only after 83 TTIs by the proposed scheduler, meaning that three users finished their transmission within the first 83 TTIs. In contrast, it took almost 150 TTIs for GPFS1 and GPFS2 to finish the transmission for three users while RRS was not able to complete the transmission for all five users within 500 TTIs.

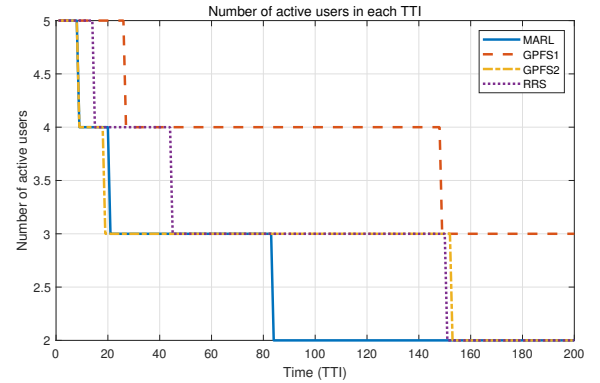


Fig. 12. Number of active users as a function of TTI.

Furthermore, we examine the total number of RBGs assigned to “UE#3”, “UE#4” and “UE#5” whose buffer sizes are 15528 bits, 4400 bits and 36400 bits, respectively. Note that the RSRP values for “UE#3”, “UE#4” and “UE#5” are -96 dB, -88 dB and -70 dB, respectively. Table VI shows the total RBG number allocated to each of these three users during the first 100 TTIs, i.e. 300 RBGs in total. We first observed that the proposed scheduler allocated more than 50%, i.e. 167 out of the total 300 RBGs to these three users of smaller buffer sizes. In addition, inspection of the simulation data revealed that it took only 9 TTIs or 16 RBGs for the proposed MARL-based scheduler to finish the transmission for “UE#4” of relatively high RSRP. Furthermore, the proposed scheduler allocated noticeably more RBGs to expediate the data transmission for “UE#3”. As a result, the proposed scheduler was able to complete the transmission for “UE#3”

TABLE VI
TOTAL RBG NUMBER ALLOCATED TO USERS OF A SMALLER BUFFER SIZE
DURING THE FIRST 100 TTIs.

	MARL	GPFS1	GPFS2	RRS
UE#3	127	75	73	84
UE#4	16	5	7	15
UE#5	24	25	20	30
Sum	167	105	100	129

after 83 TTIs, which let the network to concentrate on serving the remaining two users. By providing scheduling priority to the users of smaller buffer sizes, the proposed scheduler can improve the UDR of those users and subsequently the AUDR and 5TUDR performance.

To better characterize the proposed scheduler, we calculate the Spearman correlation coefficient matrix [24] illustrated in Fig. 13. For instance, the correlation coefficient between the allocation result of “RBG#1” and buffer is 0.6308, which implies that the allocation of “RBG#1” has a strong connection with the buffer size of the scheduled user.

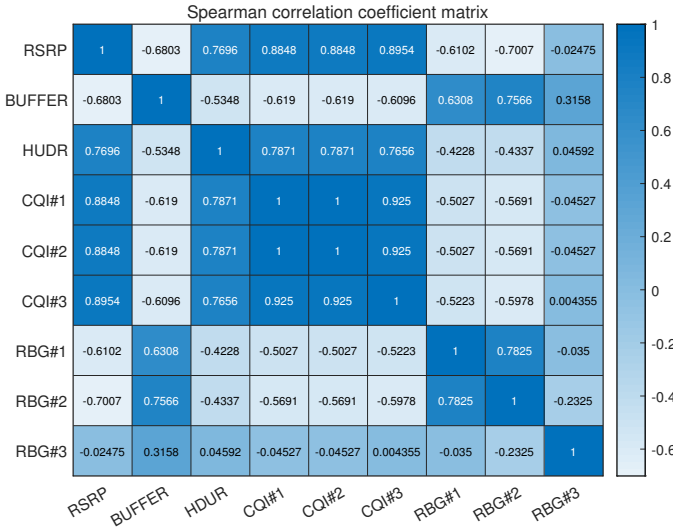


Fig. 13. Spearman correlation coefficient matrix.

In summary, the scheduling policy of the proposed MARL-based scheduler has the following characteristics. First, it prefers to distribute RBGs to different users in the same TTI. As a result, all users have more opportunities to access network resources for transmission, which effectively improves the user fairness. In addition, such a scheduling policy helps increase the average user data rate, which in turns increases the 5TUDR performance. Furthermore, the proposed scheduler is in favor of finishing the transmission requests from those users of a smaller buffer size. This feature indeed helps reduce the total time that those users spend in the network and subsequently, improve the user data rate for those users. Finally, despite that the scheduling policy of the proposed scheduler cannot be mathematically analyzed, some insights can be observed

through the Spearman correlation coefficient matrix to identify the strongly correlated input-output factor pairs.

VI. CONCLUSION

In this work, we have investigated the problem of RBG scheduling for users of bursty traffic in wireless networks. To provide fair opportunities to all users to access the available RBGs, a fairness-oriented scheduler has been formulated as a stochastic game by incorporating information from multiple network layers such as CQI and buffer size. In particular, a reward function was devised to maximize the 5%-tile user data rate. Furthermore, a MARL-based learning approach has been proposed to learn the optimal scheduling policy by dividing the large state-space into multiple sub-problems each of which is handled by one agent. Extensive computer simulation has been performed to compare the performance of the proposed scheduler against the conventional GPFS, OPS and RRS. Simulation results have confirmed that the proposed scheduler can achieve impressive 5TUDR performance while maintaining good AUDR performance. Finally, we investigated the characteristics of the scheduling policy learned by the proposed scheduler and found that the proposed scheduler distributes RBGs to more users in each TTI with higher preference towards users of a smaller buffer size.

APPENDIX

A. Network mechanism

In this appendix, we review some of the network mechanisms implemented in our network simulator that was used in generating the training and test data sets for our experiments.

1) *Out Loop Link Adaptation*: Each UE measures the received signal-to-noise ratio (SNR) on each resource block (RB), and periodically reports the corresponding CQI values to the BS. The BS selects the appropriate Modulation and Coding Scheme (MCS) based on the received CQI. However, the reported CQI is distorted by noise. As a result, the MCS chosen based on the reported CQI is not always optimal. To compensate for the discrepancy between the chosen MCS and the optimal MCS, an Out Loop Link Adaptation (OLLA) process is carried out on BS by adding a small offset α to the current CQI value q , i.e.

$$\bar{q} = [q + \alpha], \quad (27)$$

where $[\cdot]$ is the rounding operator and \bar{q} is the compensated CQI for the MCS selection. In addition, α is given by

$$\alpha = \begin{cases} \alpha + s_A, & \mathfrak{A} = 1, \\ \alpha + s_N, & \mathfrak{A} = 0, \end{cases} \quad (28)$$

where \mathfrak{A} is the corresponding ACK/NACK feedback with “1” indicating a successful transmission while “0” a failed transmission. Finally, $s_A > 0$ and $s_N < 0$ are the update rates.

2) *Transmission Block Formation*: Let $\mathcal{F}(\bar{q})$ denote the mapping from the CQI \bar{q} to its spectral efficiencies (SE), and \mathcal{I} a set of CQI levels over a specific group of RBs observed by a user. The maximum number of bits that can be loaded to this group of RBs by the user is given by

$$f(\mathcal{I}) = |\mathcal{I}| \cdot \mathcal{F} \left(\left\lfloor \frac{1}{|\mathcal{I}|} \sum_i \{\mathcal{I}\}_i \right\rfloor \right), \quad (29)$$

where $\lfloor \cdot \rfloor$ is the floor function. For instance, the estimated data rate of the n -th user in the k -th RBG can be obtained by $R_{n,k} = f(\mathcal{I}_n(k))$, where $\mathcal{I}_n(k)$ is the set of all RBs in the k -th RBG measured by the n -th user. If multiple RBGs are allocated to the same user, the same MCS is utilized to convey one transport block (TB) whose size is given by $T_n = f(\mathcal{I}_n)$, where \mathcal{I}_n is the set of all RBs allocated to the n -th user.

3) *Hybrid Automatic Repeat reQuest and Retransmission (HARQ)*: When a TB is formed, its data will be loaded into a HARQ buffer. Then, the BS will arrange at most eight HARQ processes (each with a HARQ buffer) for each TB. An ACK/NACK message will be fed back from the targeted user after a delay of seven TTIs. If an ACK message is received, the HARQ process terminates. In contrast, if a NACK message is received, a retransmission is triggered over the RBGs initially designated to the first failed transmission. As a result, those RBGs are not available for the user scheduling at the current TTI. The MCS selection and TB size remain the same for the retransmission. After five consecutive transmission failures (i.e., five NACKs), the HARQ process will expire, which causes the so-called packet loss.

B. Conventional Scheduling Schemes for Benchmarking

In this Appendix, we provide some definitions of GPFS, OPS and RRS.

1) *Generalized Proportional Fairness Scheduling (GPFS)*: In GPFS, each RBG is independently scheduled according to the Proportional Fairness (PF) values of all active users. More specifically, the PF value of the n -th user on the k -th RBG at the i -th TTI is defined as

$$\zeta_k^n[i] = \frac{(R_k^n[i])^{\alpha_1}}{(\hat{T}^n[i])^{\alpha_2}}, \quad (30)$$

where $R_k^n[i]$ is the achievable data rate of the n -th user on the k -th RBG at the i -th TTI while $\hat{T}^n[i]$ is the user's moving average throughput expressed as

$$\hat{T}^n[i] = (1 - \chi) \hat{T}^n[i - 1] + \chi T^n[i - 1]. \quad (31)$$

with χ and $T^n[i - 1]$ being the moving average coefficient and the actual TB size of the n -th user at the $(i - 1)$ -th TTI. Furthermore, α_1 and α_2 are two design parameters. For $\alpha_1 = 0$, GPFS concentrates on giving priorities to users of low average data rate in the past. In contrast, $\alpha_2 = 0$ degenerates GPFS to the conventional opportunistic scheduling.

Users of larger PF values are given higher priorities to be scheduled for the RBG under consideration.

$$P_{GPFS}^*(k) = \arg \max_n \{\zeta_k^n\}, \quad (32)$$

Note that the PF value of the same user may vary across different RBGs in the same TTI.

2) *Opportunistic Scheduling (OPS)*: The opportunistic scheduling allocates an RBG to the user who can achieve the highest estimated data rate and takes the following form:

$$P_{OP}^*(k) = \arg \max_n \{R_k^n\}. \quad (33)$$

For full buffer traffic, OPS is considered the optimal algorithm for achieving the highest network throughput and AUDR. However, this conclusion is not necessarily true for bursty traffic.

3) *Round Robin Fashion Scheduling (RRS)*: RRS is the classic scheduling algorithm that allocates all available RBGs to one user at a time and serves all users in turns. Note that new users are appended to the end of the queue for scheduling if bursty traffic is considered.

REFERENCES

- [1] S. Dang, O. Amin, B. Shihada, and M.-S. Alouini, "From a human-centric perspective: What might 6g be?," *arXiv preprint arXiv:1906.00741*, 2019.
- [2] W. Saad, M. Bennis, and M. Chen, "A vision of 6g wireless systems: Applications, trends, technologies, and open research problems," *IEEE Network*, vol. 34, no. 3, pp. 134–142, 2020.
- [3] E. L. Hahne, "Round-robin scheduling for max-min fairness in data networks," *IEEE Journal on Selected Areas in communications*, vol. 9, no. 7, pp. 1024–1039, 1991.
- [4] X. Liu, E. K. P. Chong, and N. B. Shroff, "Opportunistic transmission scheduling with resource-sharing constraints in wireless networks," *IEEE Journal on Selected Areas in Communications*, vol. 19, no. 10, pp. 2053–2064, 2001.
- [5] D. Tse, "Multiuser diversity in wireless networks," in *Wireless Communications Seminar, Stanford University*, 2001.
- [6] I.-S. Comşa, S. Zhang, M. Aydın, P. Kuonen, R. Treştian, and G. Ghinea, "A comparison of reinforcement learning algorithms in fairness-oriented ofdma schedulers," *Information*, vol. 10, no. 10, p. 315, 2019.
- [7] G. Zhu, D. Liu, Y. Du, C. You, J. Zhang, and K. Huang, "Toward an intelligent edge: wireless communication meets machine learning," *IEEE Communications Magazine*, vol. 58, no. 1, pp. 19–25, 2020.
- [8] I.-S. Comşa, S. Zhang, M. E. Aydın, P. Kuonen, Y. Lu, R. Treştian, and G. Ghinea, "Towards 5g: A reinforcement learning-based scheduling solution for data traffic management," *IEEE Transactions on Network and Service Management*, vol. 15, no. 4, pp. 1661–1675, 2018.
- [9] C. Xu, J. Wang, T. Yu, C. Kong, Y. Huangfu, R. Li, Y. Ge, and J. Wang, "Buffer-aware wireless scheduling based on deep reinforcement learning," in *2020 IEEE Wireless Communications and Networking Conference (WCNC)*, pp. 1–6, IEEE, 2020.
- [10] Y. Hua, R. Li, Z. Zhao, X. Chen, and H. Zhang, "Gan-powered deep distributional reinforcement learning for resource management in network slicing," *IEEE Journal on Selected Areas in Communications*, vol. 38, no. 2, pp. 334–349, 2019.
- [11] Y. Li, X. Fang, and S. Liang, "A novel scheduling algorithm to improve average user perceived throughput for lte systems," *IEEE Access*, vol. 7, pp. 133549–133558, 2019.
- [12] M. M. Nasralla, "A hybrid downlink scheduling approach for multi-traffic classes in lte wireless systems," *IEEE Access*, vol. 8, pp. 82173–82186, 2020.
- [13] R. Branzel, D. Dimitrov, and S. Tijs, *Models in cooperative game theory*, vol. 556. Springer Science & Business Media, 2008.
- [14] Shapley and S. L., "Stochastic games," *Proceedings of the National Academy of Sciences*, vol. 39, no. 10, pp. 1095–1100, 1953.
- [15] I. Goodfellow, Y. Bengio, A. Courville, and Y. Bengio, *Deep learning*, vol. 1. MIT press Cambridge, 2016.
- [16] R. K. Jain, D.-M. W. Chiu, W. R. Hawe, et al., "A quantitative measure of fairness and discrimination," *Eastern Research Laboratory, Digital Equipment Corporation, Hudson, MA*, 1984.
- [17] R. B. Myerson, *Game theory*. Harvard university press, 2013.

- [18] K. Cho, B. Van Merriënboer, D. Bahdanau, and Y. Bengio, "On the properties of neural machine translation: Encoder-decoder approaches," *arXiv preprint arXiv:1409.1259*, 2014.
- [19] R. Bellman, "Dynamic programming," *Science*, vol. 153, no. 3731, pp. 34–37, 1966.
- [20] C. J. Watkins and P. Dayan, "Q-learning," *Machine learning*, vol. 8, no. 3-4, pp. 279–292, 1992.
- [21] V. Mnih, K. Kavukcuoglu, D. Silver, A. Graves, I. Antonoglou, D. Wierstra, and M. Riedmiller, "Playing atari with deep reinforcement learning," *arXiv preprint arXiv:1312.5602*, 2013.
- [22] P. Sunehag, G. Lever, A. Gruslys, W. M. Czarnecki, V. F. Zambaldi, M. Jaderberg, M. Lanctot, N. Sonnerat, J. Z. Leibo, K. Tuyls, *et al.*, "Value-decomposition networks for cooperative multi-agent learning based on team reward.," in *AAMAS*, pp. 2085–2087, 2018.
- [23] M. Wunder, M. L. Littman, and M. Babes, "Classes of multiagent q-learning dynamics with epsilon-greedy exploration," in *Proceedings of the 27th International Conference on Machine Learning (ICML-10)*, pp. 1167–1174, Citeseer, 2010.
- [24] P. Sedgwick, "Spearman's rank correlation coefficient," *BMJ*, vol. 349, 2014.